Development 122, 461-472 (1996)
Printed in Great Britain © The Company of Biologists Limited 1996
DEV3339



# Specific and redundant functions of the paralogous *Hoxa-9* and *Hoxd-9* genes in forelimb and axial skeleton patterning

**Catherine Fromental-Ramain[1], Xavier Warot[1], Sudhakar Lakkaraju[1,†], Bertrand Favier[1], Herbert Haack[2], Céline Birling[1], Andrée Dierich[1], Pascal Dollé[1] and Pierre Chambon[1,*]**

[1]Institut de Génétique et de Biologie Moléculaire et Cellulaire, CNRS/INSERM/ULP, Collège de France, BP 163-67404 Illkirch-Cedex, CU de Strasbourg, France
[2]Max Planck Institute of Biophysical Chemistry, Department of Molecular Cell Biology, PO Box 2847-37018 Gottingen, Germany

*Author for correspondence
†Deceased

## SUMMARY

**Using gene targeting, we have produced mice with a disruption of *Hoxa-9* or *Hoxd-9*, two paralogous *Abdominal B*-related genes. During embryogenesis, these genes are expressed in limb buds and along the vertebral axis with anterior expression boundaries at the level of prevertebra #20 for *Hoxa-9* and #23 for *Hoxd-9*. Skeletal analysis revealed homeotic transformations corresponding to anteriorisations of vertebrae #21 to #25 (L1 to L5) in the lumbar region of *Hoxa-9*$^{-/-}$ mutants; vertebrae #23 to #25 (L3 to L5) in the lumbar region together with vertebrae #28, #30 and #31 (S2, S4 and Ca1) in the sacrum and tail were anteriorized in *Hoxd-9*$^{-/-}$ mutants. Thus, anteriorisation of vertebrae #23 to #25 were common to both phenotypes. Subtle forelimb (but not hindlimb) defects, corresponding to a reduction of the humerus length and malformation of its deltoid crest, were also observed in *Hoxd-9*$^{-/-}$, but not in *Hoxa-9*$^{-/-}$, mutant mice. By intercrosses between these two lines of mutant mice, we have produced *Hoxa-9/Hoxd-9* double mutants which exhibit synergistic limb and axial malformations consisting of: (i) an increase of penetrance and expressivity of abnormalities present in the single mutants, and (ii) novel limb alterations at the level of the forelimb stylopod and additional axial skeleton transformations. These observations demonstrate that the two paralogous genes *Hoxa-9* and *Hoxd-9* have both specific and redundant functions in lumbosacral axial skeleton patterning and in limb morphogenesis at the stylopodal level. Taken all together, the present and previously reported results show that disruption of different *Hox* genes can produce similar vertebral transformations, thus supporting a combinatorial code model for specification of vertebral identity by *Hox* genes.**

Key words: paralogous *Hox* genes, gene disruption, pattern formation, combinatorial code, mouse, *Hoxa-9*, *Hoxd-9*

## INTRODUCTION

The murine genome contains 38 homeobox-containing genes (*Hox* genes) which are related to *Drosophila* homeotic genes and clustered in four chromosomal loci, the *HOXA*, *B*, *C* and *D* complexes (for review see McGinnis and Krumlauf, 1992). These complexes, whose organization has been highly conserved during vertebrate evolution, were most probably generated by quadruplication of an ancestral complex during early chordate evolution (Ruddle et al., 1994). Homeodomain sequence comparisons led to a classification of *Hox* genes in 13 subfamilies or homology groups (Scott, 1992). Each subfamily contains 2-4 highly related paralogous genes which are similarly located within their respective complexes. As in Drosophila, the chromosomal order of the mouse *Hox* genes is colinear to the relative position of their expression domains along the anteroposterior (A-P) axis of the developing embryo, such that the more 3′ the gene is located, the more anterior is its expression boundary. The temporal activation of *Hox* genes is also related to their location in the complex, the most 3′ genes being expressed earlier. These properties are referred to as the 'spatiotemporal colinearity' (For review, see Dollé and Duboule, 1993). Interestingly, similar properties have been described for genes located in the 5′ regions of the *HOXA*, *C* and *D* complexes during pattern formation in the mouse along appendicular structures such as the limb buds (Dollé et al., 1989; Haack and Gruss, 1993; Peterson et al., 1994) and genital tubercule (Dollé et al., 1991). Indeed, the *Hoxd-9* to *Hoxd-13* and *Hoxa-9* to *Hoxa-13* genes display nested and colinear expression domains in the mesenchyme of the developing limb buds resulting from the successive activation of these genes, the expression boundaries of *Hoxa* genes being slightly distinct from those of their *Hoxd* paralogs (see Fig. 1A).

The colinear *Hox* gene expression patterns have led to the hypothesis that these genes may specify regional identity along the main body axis and along appendicular structures, and that paralogous genes may have partly overlapping (redundant) functions (for review see Krumlauf, 1994). This hypothesis has

been supported by the analysis of mice with either gain-of-function or loss-of-function of *Hox* genes. Gain-of-function experiments involving the ectopic expression of a given *Hox* gene often result in morphological transformations toward the aspect of a structure that normally expresses this gene (Kessel et al., 1990; Morgan et al., 1992; Lufkin et al., 1992). Loss-of-function mutant mice show either regional loss of structures or localized homeotic transformations along the A-P axis (see Krumlauf, 1994, and references therein). Moreover, disruptions of the *Hoxa-11* (Small and Potter, 1993), *Hoxd-11* (Davis and Capecchi, 1994; Favier et al., 1995) and *Hoxd-13* (Dollé et al., 1993) genes affect restricted regions of both the axial and limb skeleton.

The mouse *Hoxa-9* and *Hoxd-9* genes are the most 3′ located genes among the set of *Hoxa* and *Hoxd* genes phylogenetically related to the *Drosophila Abdominal B* homeotic gene (see Fig. 1A). They are expressed both along the primary body axis, e.g. in the spinal cord and prevertebral column, and in the developing limbs (Duboule and Dollé, 1989; Haack and Gruss, 1993). In the prevertebral column of 12.5 days post-coitum (dpc) fetuses, the rostral expression boundary of *Hoxd-9* is in prevertebra #23, the 3rd lumbar prevertebra, with a weak expression detected up to prevertebra #21, whereas the expression of *Hoxa-9*, which is strong up to prevertebra #20 and weaker up to prevertebra #17, extends along the ventral side of the prevertebrae up to prevertebra #14 (Duboule and Dollé, 1989; our unpublished data; see also Fig. 9).

We have now generated mouse lines with targeted disruption of either *Hoxa-9* or *Hoxd-9* to investigate their possible patterning role along the developing rostrocaudal axis and limbs. Mice homozygous for the *Hoxa-9* mutation exhibit anterior homeotic transformations in the lumbar region (L1 to L5) of the vertebral column. The *Hoxd-9* mutation also results in anterior transformations in the lumbar region (although less extended, L3 to L5) and in the sacral region (S2 and S4, Ca1), as well as in regional alterations of the proximal portion of the forelimb. In addition, the analysis of *Hoxa-9/Hoxd-9* double mutant mice obtained by intercrosses reveals a partial functional redundancy between these two genes along the A/P axis, as well as in the forelimb.

## MATERIAL AND METHODS

### Construction of targeting vectors

A 4.4 kb *Eco*RI 129/Sv genomic fragment containing the *Hoxa-9* gene was subcloned into the pTZ plasmid (Pharmacia) where the *Hin*dIII site is missing. A 1.5 kb *Bgl*II PGK-Neo cassette, purified from the PD350.1 plasmid (a gift from D. Lohnes, Rijli et al., 1994), was inserted in the same transcriptional orientation as *Hoxa-9*, into the *Bgl*II site of the homeobox. This insertion interrupts the *Hoxa-9* protein sequence at the level of aminoacid 47 of the homeodomain which corresponds to the first quarter of the α-helix 3 (the DNA recognition helix). The resulting targeting vector pTa9PGKneo (see Fig. 1C) was linearized (at the 5′ extremity of the genomic DNA) by *Kpn*I prior to its introduction into D3 embryonic stem (ES) cells (Gossler et al., 1986) by electroporation.

An 8 kb *Kpn*I-*Xho*I genomic fragment, containing the *Hoxd-9* gene, was subcloned in the Bluescript plasmid (Stratagene) from a 129/Sv genomic cosmid CosN (Duboule and Dollé, 1989) provided by D. Duboule. A PGK-TK cassette, purified from plasmid pD352 (a gift from D. Lohnes, Rijli et al., 1994), was inserted at the 5′ extremity of the genomic fragment. A PGK-Neo (Rijli et al., 1994) or MC1-Neo cassette (Thomas and Capecchi, 1987, a gift from M. Capecchi) was subcloned in the *Eco*RI site of the *Hoxd-9* homeobox yielding the pTKd9PGKneo (see Fig. 1B) or pTKd9MC1neo constructs, respectively. The *Hoxd-9* open reading frame is thus interrupted at the level of the 18th aminoacid of the homeodomain (e.g. in the middle of the first helix). These vectors were linearized by *Xho*I digestion before electroporation of D3 ES cells (Gossler et al., 1986).

### Identification of the targeted ES cell clones

Electroporations and ES cell culture were performed as described (Dollé et al., 1993) and targeted clones were identified by Southern blot analysis.

(1) For *Hoxd-9* (see Fig. 1B). The 5′ external probe A, a 580 bp *Bgl*II-*Kpn*I fragment, was used with ES cell DNA digested by *Bgl*II. This probe hybridized to a 9.5 kb wild-type (WT) fragment and to a 11 kb DNA fragment for the mutant allele. Southern analysis of genomic DNA digested by *Not*I and hybridized with the 3′ external probe B (a 1 kb *Bst*XI fragment) showed an 8.6 kb band for the WT allele and a 10 kb band for the mutant allele.

(2) For *Hoxa-9* (see Fig. 1C). The 3′ external probe E (see Fig. 1C), a 1.4 kb *Eco*RI genomic fragment was used for Southern analysis of ES cells DNA digested by *Bam*HI. The DNA fragment hybridizing to probe E is about 8.8 kb for the WT allele and 5 kb for the mutant allele. Probe E was also used on genomic DNA digested by *Kpn*I to confirm the presence of the mutation by hybridizing to a 9.4 kb fragment for the WT allele and a 10.8 kb fragment for the mutated allele.

In both cases, a neomycin probe and internal genomics probes (probe C, a 0.8 kb *Pst*I-*Eco*RI fragment, for *Hoxd-9* and probe D, a 1.5 kb fragment, for *Hoxa-9*) were used to discriminate ES cell clones containing random insertion of the plasmid.

Electroporation experiments, each with $10^7$ D3 ES cells were performed and resulted for *Hoxa-9* in 2 targeted ES cell clones out of 85 neomycin-resistant clones and for *Hoxd-9* in 1 targeted ES cell clone out of 17 for the pTKd9PGKneo vector and 2 out of 55 for the pTKd9MC1neo vector.

### Establishment of the mutant lines

Upon blastocyst injection, all these clones yielded germline-transmitting male chimeras. These chimeras were crossed with 129/Sv or C57Bl/6 females to produce heterozygous mutants in inbred (129/Sv) or mixed (129/Sv-C57Bl/6) genetic backgrounds, respectively. Mutant and littermate control animals were killed at birth or at 1 to 6 months post-partum and alcian blue/alizarin red skeletal staining was performed as described (Dollé et al., 1993).

## RESULTS

### Targeted disruptions of the *Hoxd-9* and *Hoxa-9* genes are not lethal

For each gene, two independent ES cell clones were successfully targeted with constructs disrupting the homeobox (see Fig. 1B,C, and Materials and Methods). These clones were injected into recipient blastocysts and, for each gene, both clones gave at least 3 chimeric males transmitting the mutated allele to their progeny.

*Hoxd-9*$^{+/-}$ and *Hoxa-9*$^{+/-}$ mice appeared externally normal and were fertile. The progenies obtained from heterozygote intercrosses showed a Mendelian ratio of homozygous mutant/heterozygous/WT animals (1:2:1). Homozygous *Hoxa-9*$^{-/-}$ and *Hoxd-9*$^{-/-}$ animals were externally indiscernible from their littermates and had a normal life span. Mutant females gave birth to regular size litters. The results described hereafter

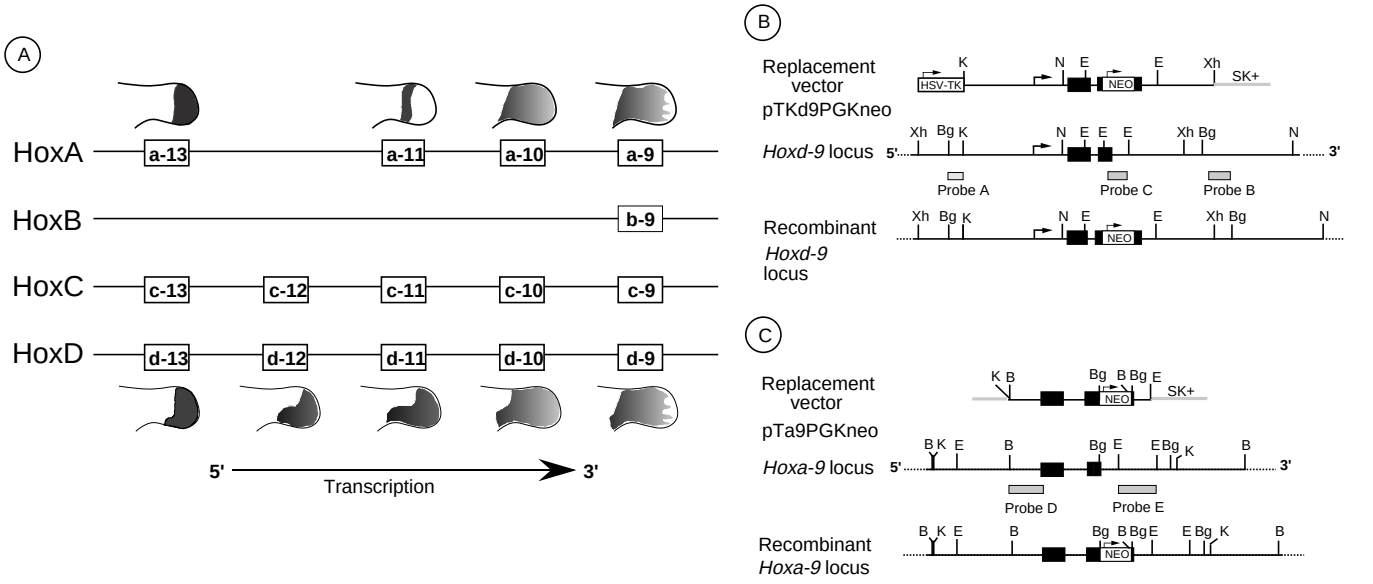


**Fig. 1**. (A) Schematic representation of the expression domains of the *Abdominal B*-related *Hoxa* and *Hoxd* genes in mouse limb bud at approximately 11. 5 dpc. The 5′ parts of the *HOXA*, *B*, *C* and *D* complexes are shown and the genes are indicated by open boxes. The common orientation of transcription is indicated below. (B,C) Gene targeting of *Hoxd-9* and *Hoxa-9*. Restriction maps describing the structures of the targeting vectors (upper), the WT genomic locus (middle) and the recombinant locus (lower) for *Hoxd-9* (B) and *Hoxa-9* (C). The positions of the 5′ external, internal and 3′ external probes for Southern blot analysis are indicated under the WT locus for each gene. Abbreviations: B, *Bam*HI; Bg, *Bgl*II; E, *Eco*RI; K, *Kpn*I; N, *Not*I; Xh, *Xho*I, SK+, vector sequence (pBluesriptSK+, Stratagene)

were obtained for mice with a C57Bl/6 × 129/Sv hybrid genetic background or a pure 129/Sv background.

## Axial skeleton homeosis

### (1) Anterior transformations of lumbar vertebrae in *Hoxa-9*$^{-/-}$ mutant mice

The *Hoxa-9*$^{-/-}$ mutation resulted in a series of vertebral anteriorisations in the lumbar region. The most obvious feature was the presence of a supernumerary pair of ribs on vertebrae #21 (position of the L1 in WT animal, noted hereafter WT L1) which, together with the absence of the transverse processes, corresponds to a transformation of the first lumbar vertebra towards a thoracic vertebral morphology (Fig. 2C, T13*; see also Figs 3, 9). These extra ribs, observed in all examined animals, were shorter than the 13th pair of ribs and oriented more posteriorly. Additional anteriorisations were observed along the lumbar region down to vertebra #25 (WT L5) (see Figs 3, 9). The *Hoxa-9*$^{-/-}$ vertebra #25 (WT L5) had small tips resembling the accessory processes of WT L4 vertebrae, whereas the mutant #24 vertebrae (WT L4) exhibited an extended accessory process which is observed in WT down to L3 only (Fig. 3, L3*, curved arrow). The accessory processes of mutant #23 vertebra (WT L3) were shorter than those of WT L3 vertebrae, thus resembling those of WT L2 vertebrae. The mutant vertebrae #22 (WT L2), #23 (WT L3) and #24 (WT L4) had lateral processes (straight arrows in Fig. 3) whose size and orientation were similar to those of WT L1, L2 and L3 vertebrae, respectively. These transformations,

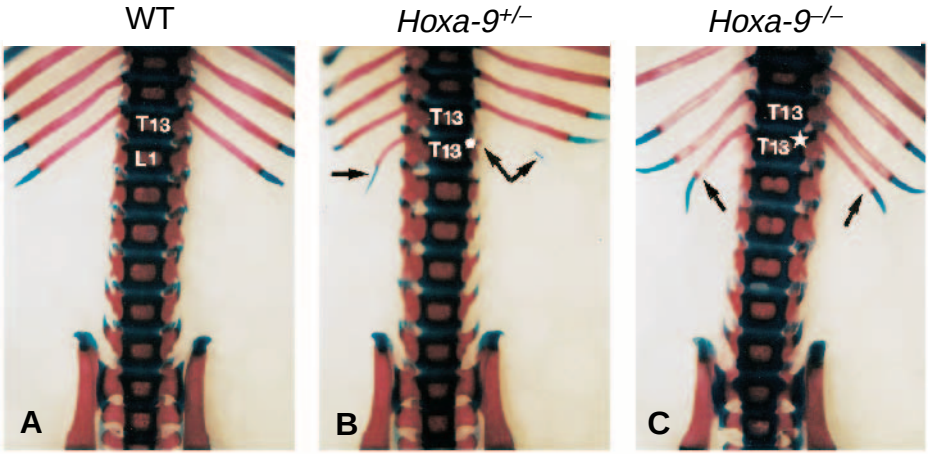


**Fig. 2**. Comparison of alcian blue/alizarin red-stained lumbar vertebral regions of 2-day-old littermate animals with a WT (A), *Hoxa-9*$^{+/-}$ (B) or *Hoxa-9*$^{-/-}$ (C) genotype. Note in B the small supernumerary extra rib on the right side of T13• (partially transformed L1 vertebra) and cartilage and bone rib rudiments on the left side of T13• (arrows). Note in C the presence of two entire extra ribs on T13* (fully transformed L1 vertebra). L, lumbar vertebra; T, thoracic vertebra.

which were observed in all the 20 *Hoxa-9*$^{-/-}$ mutants examined, were not seen in any of the 8 littermate WT mice analyzed. In contrast, the morphology and size of vertebra #26 (WT L6) was normal in *Hoxa-9*$^{-/-}$ mutants, indicating the posterior limit of the transformations induced by this mutation (data not shown). No significant modifications could be observed in the thoracic region.

### (2) Anterior transformations of lumbar and sacral vertebrae in *Hoxd-9*$^{-/-}$ mutant mice

85% of the *Hoxd-9*$^{-/-}$ mutant mice (29 animals examined) exhibited anteriorisation of some vertebrae in the lumbar region. The morphology of mutant vertebrae #23, #24 and #25 (WT L3, L4 and L5) resembled that of L2, L3 and L4 WT vertebrae (see Fig. 3, L2*, L3* and L4*, respectively, and Fig.

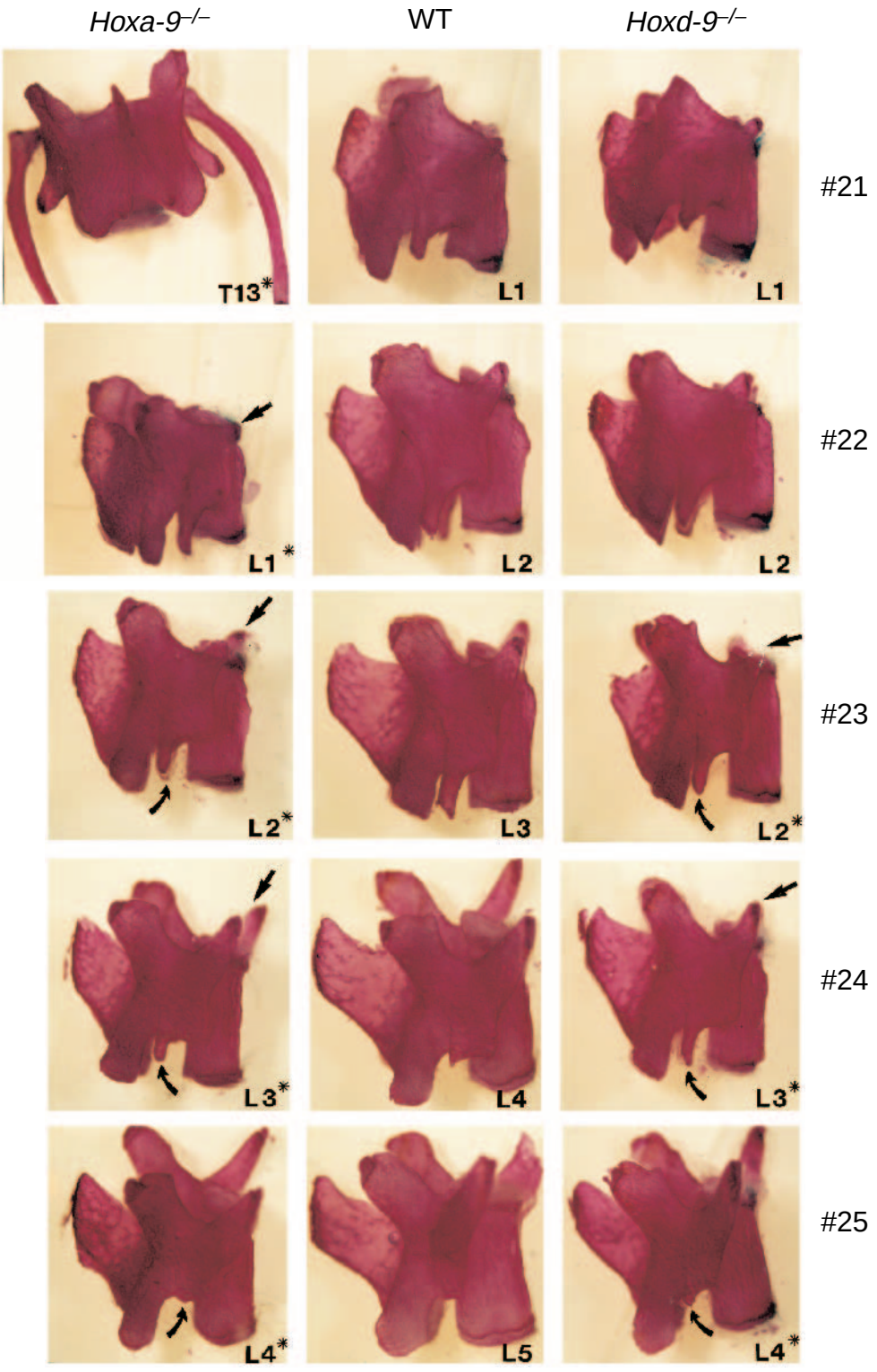


**Fig. 3**. Anterior homeosis of lumbar vertebrae in *Hoxa-9*$^{-/-}$ and *Hoxd-9*$^{-/-}$ mutants. Right side views of alizarin red-stained dissected lumbar vertebrae of a control wild-type animal (WT), a *Hoxa-9*$^{-/-}$ and a *Hoxd-9*$^{-/-}$ homozygote mice at the same age (2-month-old). The WT and the *Hoxd-9*$^{-/-}$ animals are littermates. The mutant vertebrae are indicated with an asterisk when they display a transformed morphology. For instance, the *Hoxa-9*$^{-/-}$ mutant T13* to L4* are the counterparts of WT L1 to L5, respectively. Each mutant vertebra should thus be compared both to its WT counterpart and to the next anterior WT vertebra. The numbers on the right side of the figure correspond to the position of the vertebrae along the vertebral column. Notice the following signs of transformation for *Hoxa-9*$^{-/-}$ vertebrae: the appearance of an extra pair of ribs on vertebra #21 (T13*), the change of orientation of the lateral processes of vertebra #22 (L1*), the abnormal size of the lateral and accessory processes of the vertebrae #23 and #24 (L2* and L3*) and the appearance of a small tip as an accessory process on vertebra #25 (L4*). The same signs of anteriorisation can be observed for vertebrae #23, #24 and #25 (L2*, L3* and L4*) in the *Hoxd-9*$^{-/-}$ mutants. The straight arrows and the curved arrows point to the lateral processes and the accessory processes of the vertebrae, respectively. L, lumbar vertebra; T, thoracic vertebra.

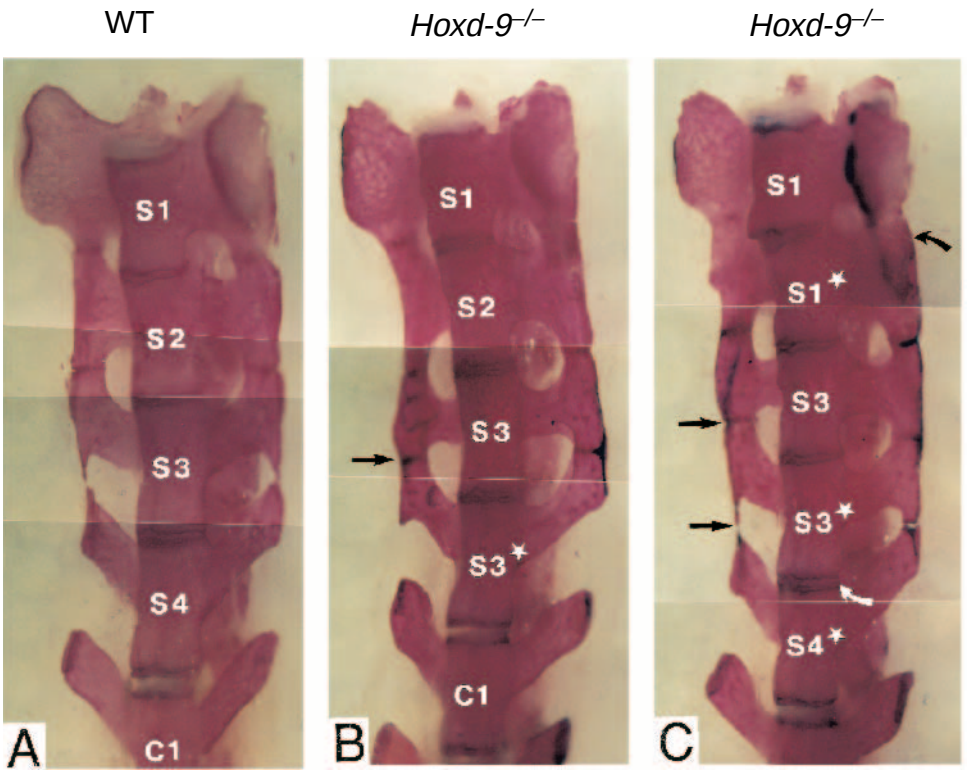


**Fig. 4**. Comparison of alizarin red-stained sacral and first caudal vertebrae from a WT animal (A) and two *Hoxd-9*$^{-/-}$ mutant specimens (B,C) at the same age (2-month-old). The mutant vertebrae are indicated with an asterisk when displaying a transformed morphology. (B) The morphology of the 4th sacral vertebra (S3*) is altered, its transverse processes being completely fused to those of S3 (black arrow). (C) Note that the phenotype of the specimen here is stronger, as in addition the 2nd sacral vertebra (S1*) exhibits an abnormal articular surface for the ilium bone (curved arrow) and the 1st caudal vertebra (S4*) has its transverse processes partially connected to those of its anterior neighbour (S3*) (black arrow) and its vertebral body fused to that of S3* (white arrow). Note also the more pronounced reduction in size of the sacral and caudal vertebrae from the mutant animal in C. S, sacral vertebra; C,caudal vertebra.

9). No signs of transformation of mutant vertebrae #21 (WT L1), #22 (WT L2) and #26 (WT L6) could be observed. The remaining 15% *Hoxd-9*$^{-/-}$ mutants exhibited only unilateral transformations of vertebrae #23, #24 and #25 (not shown).

The *Hoxd-9*$^{-/-}$ mutants also displayed anteriorisation of some sacral vertebrae. In 30% of the *Hoxd-9*$^{-/-}$ mutants, the articular surface of the ilium extended bilaterally on vertebra #27 (WT S1) and vertebra #28 (WT S2) (see Fig. 4C S1*, curved arrow) instead of being limited to S1 as in the WT sacrum. Therefore, the mutant vertebra #28 takes, with a partial penetrance, an S1 morphology. 95% of the *Hoxd-9*$^{-/-}$ mice had their vertebra #30 (WT S4) completely fused to vertebra #29 (WT S3) by their transverse processes (see Fig. 4B,C, S3*, straight arrows). Such a fusion is seen in WT between S3 and S2, S4 remaining apart (Fig. 4A). In a number of cases, the *Hoxd-9*$^{-/-}$ vertebra #31 (WT Ca1) exhibited an S4 morphology, with transverse processes and vertebral body partly fused to those of its anterior neighbour (Fig. 4C, S4*, curved white arrow). Note that the vertebra #27 (WT S1) of *Hoxd-9*$^{-/-}$ mutants was never transformed into a L6 morphology, and that no differences could be observed between mutant and WT vertebrae #26 (WT L6). Thus, mutant vertebrae #28, #30 and #31 appeared to be anteriorly transformed with a variable penetrance into vertebrae exhibiting characteristics of WT S1, S3 and S4, respectively (see also Fig. 9). Some *Hoxd-9*$^{-/-}$ mutants also presented a decrease in the size of their sacral region, the shortening being accentuated when the phenotype was stronger (compare Fig. 4A, B and C).

### (3) Partial anterior transformations of lumbar vertebrae in *Hoxa-9*$^{+/-}$ and *Hoxd-9*$^{+/-}$ heterozygous single mutants

Partial anterior transformations were observed in the lumbar region of 60% of *Hoxa-9*$^{+/-}$ mutant mice (18 animals examined). These mutants exhibited partial, and sometimes asymmetric, rib rudiments (bony and/or cartilaginous part of the rib) with occasionally a full unilateral rib on vertebra #21 (WT L1) (see Fig. 2B, T13• and data not shown). Unilateral or bilateral transformations of vertebrae #22 to #25 (WT L2 to L5) were also observed in these heterozygous mutant animals (data not shown). The remaining 40% of *Hoxa-9*$^{+/-}$ mutants harboured the lumbar vertebral pattern of WT animals.

50% of the *Hoxd-9*$^{+/-}$ mice (21 animals studied) also exhibited unilateral (40%) or sometimes bilateral (10%) partial anteriorisation of vertebrae #23 (WT L3), #24 (WT L4) and #25 (WT L5) (data not shown). Interestingly, the unilateral transformations were preferentially seen on the left side of the vertebrae as previously observed in the case of *Hoxd-11*$^{-/-}$ mutants (Favier et al., 1995). Abnormal fusions between vertebrae #29 (WT S3) and #30 (WT S4) were present in 40% of the *Hoxd-9*$^{+/-}$ mutants (data not shown).

### (4) Double *Hoxa-9/Hoxd-9* mutants

Previous studies have suggested that paralogous genes could be at least partially functionally redundant (Condie and Capecchi, 1994; Davis et al., 1995). To investigate whether a similar redundancy may exist between *Hoxa-9* and *Hoxd-9*, double mutant mice were generated by crossing *Hoxa-9*$^{-/-}$ and *Hoxd-9*$^{-/-}$ founders. The resulting double heterozygous (*Hoxa-9*$^{+/-}$/*Hoxd-9*$^{+/-}$) mice were viable and fertile and, by intercrosses, produced mice with all possible genotype combinations at the expected frequencies. All of these mice were viable and fertile, although the fertility of the double homozygous mutant animals was low. Indeed, only 5 males out of 10 tested and 5 females out of 11 tested, appeared to be fertile, and the

females gave birth to abnormally small litters, with never more than 3 pups which often died after one day.

*Hoxa-9*$^{+/-}$*/Hoxd-9*$^{+/-}$ double mutants exhibited a vertebral phenotype which was not more severe than that of the corresponding heterozygous single mutants. Partial anterior transformations of vertebrae #21 to #25 (WT L1 to L5), resembling WT T13, L1, L2, L3 and L4 vertebrae, respectively, were observed, thus mimicking the *Hoxa-9*$^{+/-}$ phenotype (compare Fig. 5C with Fig. 2B, and data not shown).

*Hoxa-9*$^{-/-}$*/Hoxd-9*$^{-/-}$ double mutants exhibited a 14th pair of ribs on vertebra #21 (WT L1, transformed into T13*) followed posteriorly by six lumbar (L1* to L6*) and four sacral (S1* to S4*) vertebrae of apparently normal morphology (Fig. 5F, and data not shown; see also Fig. 9). These lumbar and sacral vertebrae extended from vertebrae #22 to #31 instead of vertebrae #21 to #30 in WT animals. This phenotype is interpreted as a series of anterior transformations along the A-P axis starting from vertebra #21 (WT L1) and extending to at least vertebra #32 (WT Ca2), identification of more posterior vertebrae being difficult. Hence, the double homozygous mutants exhibited a transformed phenotype which was more severe than that expected from the simple addition of each single mutant phenotype. Indeed, vertebrae #26 (WT L6), #27 (WT S1) and #29 (WT S3), which were not affected in the single mutant mice, were anteriorised in *Hoxa-9*$^{-/-}$*/Hoxd-9*$^{-/-}$ mutants.

In *Hoxa-9*$^{-/-}$*/Hoxd-9*$^{-/-}$ double mutants, the anterior transformations of vertebra #27 (WT S1) and #28 (WT S2) to L6* and S1*, respectively, induced a posterior shift of the vertebral articular surface with the ilium bone from vertebra #27 to #28. However, the whole hindlimb is only shifted posteriorly by half a vertebra since the articulation (joining the S1* vertebra to the ilium bone) is posteriorly displaced on the ilium bone surface. This compensates for half of the posterior shift of the S1 morphology and makes L6* completely surrounded by the ilium (compare Fig. 5A and F, or left and right side in Fig. 5G).

Interestingly, the vertebral phenotypes of *Hoxa-9*$^{+/-}$*/Hoxd-9*$^{-/-}$ or

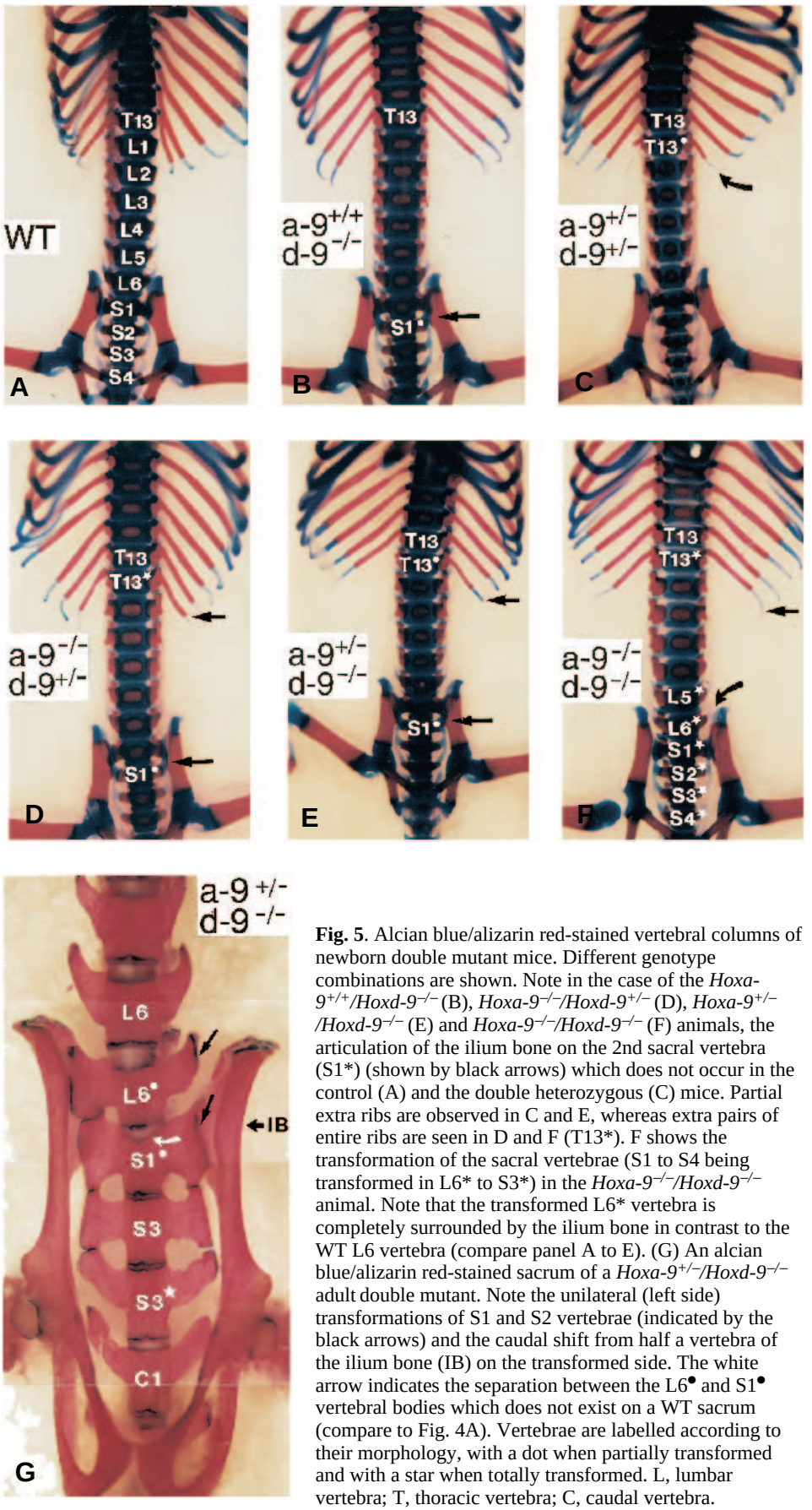


**Fig. 5**. Alcian blue/alizarin red-stained vertebral columns of newborn double mutant mice. Different genotype combinations are shown. Note in the case of the *Hoxa-9*$^{+/+}$*/Hoxd-9*$^{-/-}$ (B), *Hoxa-9*$^{-/-}$*/Hoxd-9*$^{+/-}$ (D), *Hoxa-9*$^{+/-}$*/Hoxd-9*$^{-/-}$ (E) and *Hoxa-9*$^{-/-}$*/Hoxd-9*$^{-/-}$ (F) animals, the articulation of the ilium bone on the 2nd sacral vertebra (S1*) (shown by black arrows) which does not occur in the control (A) and the double heterozygous (C) mice. Partial extra ribs are observed in C and E, whereas extra pairs of entire ribs are seen in D and F (T13*). F shows the transformation of the sacral vertebrae (S1 to S4 being transformed in L6* to S3*) in the *Hoxa-9*$^{-/-}$*/Hoxd-9*$^{-/-}$ animal. Note that the transformed L6* vertebra is completely surrounded by the ilium bone in contrast to the WT L6 vertebra (compare panel A to E). (G) An alcian blue/alizarin red-stained sacrum of a *Hoxa-9*$^{+/-}$*/Hoxd-9*$^{-/-}$ adult double mutant. Note the unilateral (left side) transformations of S1 and S2 vertebrae (indicated by the black arrows) and the caudal shift from half a vertebra of the ilium bone (IB) on the transformed side. The white arrow indicates the separation between the L6• and S1• vertebral bodies which does not exist on a WT sacrum (compare to Fig. 4A). Vertebrae are labelled according to their morphology, with a dot when partially transformed and with a star when totally transformed. L, lumbar vertebra; T, thoracic vertebra; C, caudal vertebra.

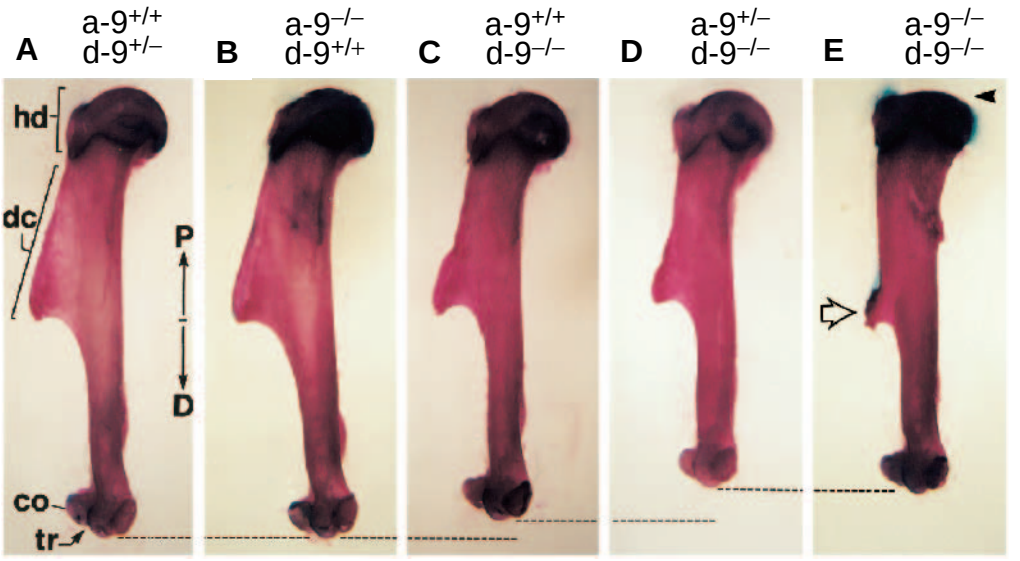


**Fig. 6**. Comparison of the humerus of control (A) or various simple or double *Hoxa-9* and/or *Hoxd-9* mutant mice (B-E) as indicated. Notice (i) the increasing degree of size reduction and (ii) the proximal morphological alterations in C-E. The arrowhead shows the severely flattened humeral head and the open arrow indicates a 'remnant' of the deltoid tuberosity in the double homozygous null mutant. co, condyle; dc, deltoid crest; hd, head of the humerus; tr, trochlea; P/D, proximal/distal.

*Hoxa-9*$^{-/-}$/*Hoxd-9*$^{+/-}$ double mutants were sometimes more severe than expected from the simple addition of the corresponding single mutant phenotypes. Only 30% of the *Hoxa-9*$^{+/-}$/*Hoxd-9*$^{-/-}$ mutants exhibited the sum of *Hoxd-9*$^{-/-}$ and *Hoxa-9*$^{+/-}$ mutant phenotypes, whereas 50% of them displayed the same phenotype as homozygous double mutants, and the remaining 20% exhibited unilateral anterior transformations (preferentially on the left side) of vertebra #26 (WT L6) to L5*, of vertebra #27 (WT S1) to L6* and of vertebra #28 (WT S2) to S1* (see Fig. 5G and Fig. 9). Similarly, 60% of *Hoxa-9*$^{-/-}$/*Hoxd-9*$^{+/-}$ mutants showed the vertebral phenotype of *Hoxa-9*$^{-/-}$ mutants, whereas 40% of them displayed the phenotype of the homozygous double mutants.

## Limb abnormalities

The limbs of either *Hoxa-9*$^{-/-}$ or *Hoxd-9*$^{-/-}$ single mutant mice appeared externally normal (data not shown). Alizarin red/alcian blue stainings showed no detectable alteration of the limb skeleton in *Hoxa-9*$^{-/-}$ mutants, either in newborns or adults (data not shown). In particular, the humerus of *Hoxa-9*$^{-/-}$ mutants appeared normal in size and shape (Fig. 6B, and data not shown). Only mild humeral alterations were found in *Hoxd-9*$^{-/-}$ mutants. The entire humerus was slightly shortened (8 to 10% reduction of its proximodistal (P-D) length). The deltoid crest was variably underdeveloped in different *Hoxd-9*$^{-/-}$ mutants (Fig. 6C, and data not shown). Other parts of the humerus, including the humeral head, were normal in *Hoxd-9*$^{-/-}$ mutants (Fig. 6C).

The examination of both *Hoxa-9* and *Hoxd-9* compound mutants revealed clear, dose-dependent, 'synergistic' alterations in the proximal forelimb skeleton. *Hoxa-9*$^{-/-}$/*Hoxd-9*$^{-/-}$ double mutant mice always displayed (i) a marked P-D shortening of the humerus and (ii) severe proximal alterations of this bone. The humerus bones were bilaterally 15-20% shorter than those of WT littermates (Fig. 6E). This length reduction was already present in 2-day-old animals (data not shown). Interestingly, the entire humerus was shortened, even though the proximal half only was altered in shape (Fig. 6E). Indeed, the deltoid crest was severely affected. In most instances, it was completely absent,

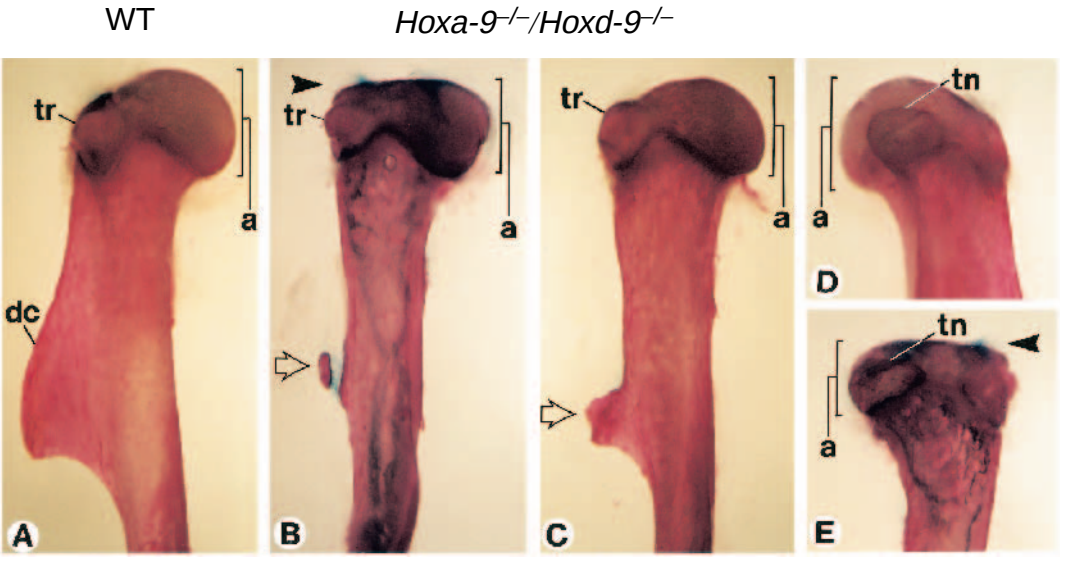


**Fig. 7**. The double *Hoxa-9*$^{-/-}$/*Hoxd-9*$^{-/-}$ mutant humeral phenotype. (A-C). Caudolateral views of the proximal part of a WT (A) and two double null mutant (B,C) humerus. (D, E) Craniomedial views of the humeral heads of the specimens shown in A and B, respectively. The open arrows point to the small bony rudiments reminiscent of deltoid tuberosities in mutant specimens, and the arrowheads show the severely flattened humeral head. a, articular surface of the humeral head; dc, deltoid crest; tn, trochin (tuberculum minus); tr, trochiter (tuberculum majus).

**Table 1. Specification of lumbo-sacral-caudal vertebrae**

| Vertebra identity | Hox genes involved from single or double mutations (a) | Redundant Hox genes from double mutations (a) |
|---|---|---|
| #21 (WT L1) | a-9, a-10, c-9 (b) | |
| #22 (WT L2) | a-9, a-10 | |
| #23 (WT L3) | a-9, d-9, a-10 | |
| #24 (WT L4) | a-9, d-9, a-10 | |
| #25 (WT L5) | a-9, d-9, a-10, d-11 | a-10/d-11** |
| #26 (WT L6) | a-9*, d-9*, a-10, d-11 | a-9/d-9; a-10/d-11** |
| #27 (WT S1) | a-9*, d-9*, a-10*, d-11 | a-9/d-9; a-10/d-11** |
| #28 (WT S2) | a-9*, d-9, a-10*, d-11 | a-9/d-9**; a-10/d-11** |
| #29 (WT S3) | a-9*, d-9*, a-10*, d-11 | a-9/d-9; a-10/d-11** |
| #30 (WT S4) | d-9, a-10*, d-11, d-13 | a-10/d-11** |
| #31 (WT Ca1) | a-9*, d-9, a-10*, d-11 | a-9/d-9**; a-10/d-11** |
| #32 (WT Ca2) | a-9*, d-9*, a-10*, d-11 | a-9/d-9; a-10/d-11* |

*No anterior transformation when singly mutated.
**Indicates partial redundancy between the two Hox genes.
(a) For references, see Fig. 9.
(b) See Suemori et al. (1995).
The transformations observed in Hoxa-11 (Small and Potter, 1993) and Hoxa-11/Hoxd-11 (Davis et al., 1995) mutant mice are not included in this table, because the morphology of the transformed lumbar vertebrae was not described in these studies.

except for a distal rudiment consisting either of a small floating bone (Fig. 7B) or a bony protrusion (Figs 7C, 6E). In a few double mutants, the deltoid crest existed, but was severely truncated (data not shown). The shape of the humeral head was also affected in *Hoxa-9*$^{-/-}$*/Hoxd-9*$^{-/-}$ mutants. In some specimens, the head was severely flattened, but the two major tuberosities, the trochiter and trochin, could still be identified (Fig. 7B,E). Most of the double mutants, however, showed milder truncations of the humeral head articular surface (Fig. 6E). It is noteworthy that deformations of the humeral head were already visible in 2 day-old newborn mice at a time where the humeral epiphysis was still cartilaginous (data not shown).

In contrast, there was no deformation of the distal part of the humerus in *Hoxa-9*$^{-/-}$*/Hoxd-9*$^{-/-}$ double mutants (Figs 6E, 8B,C, and data not shown). Nevertheless, several double mutants had ectopic sesamoid bones in the elbow region. Normal mice have a single sesamoid bone at the lateral side of the elbow (Fig. 8A, white asterisk). Out of 14 *Hoxa-9*$^{-/-}$*/Hoxd-9*$^{-/-}$ mutant limbs examined, 5 displayed a small supernumerary bone on the lateral side (Fig. 8B, curved arrow), and 5 had a supernumerary sesamoid on the medial side (not shown). In addition, two mutants had a large supernumerary sesamoid along the cranial side of the elbow joint (Fig. 8C, black arrows, D). These ectopic bony structures may correspond to abnormal ossifications in tendons or in the articular capsule caused by impairments of the elbow mobility. This may either result from subtle, undetected alterations to the distal extremity of the humerus, or simply be a consequence of the humeral shortening. There was no detectable alteration in the radius, ulna or more distal forelimb bones in *Hoxa-9*$^{-/-}$*/Hoxd-9*$^{-/-}$ mutants.

Interestingly, the *Hoxa-9* mutation behaved as a semi-dominant mutation in the *Hoxd-9*$^{-/-}$ background. Indeed, *Hoxa-9*$^{+/-}$*/Hoxd-9*$^{-/-}$ mutants had a humeral length shortening (12-15%) which was between that of *Hoxd-9*$^{-/-}$ simple mutants and *Hoxa-9*$^{-/-}$*/Hoxd-9*$^{-/-}$ double homozygotes (Fig. 6D). The same mutant mice usually had deltoid crests which were more affected than in *Hoxd-9*$^{-/-}$ single mutants (compare Fig. 6D to C), and thus resembled those of mildly affected double homozygous mutants. *Hoxa-9*$^{+/-}$*/Hoxd-9*$^{-/-}$ mutants also displayed occasional supernumerary elbow sesamoids similar to those described above (data not shown).

The opposite genotype combination, *Hoxa-9*$^{-/-}$*/Hoxd-9*$^{+/-}$, resulted in humerus bones which were normal in size and shape (data not shown).

None of the double mutants exhibited any alterations in the hindlimbs.

## DISCUSSION

We have generated *Hoxa-9* and *Hoxd-9* single and double mutants to investigate the role of these genes during mouse development. Both anterior homeosis of vertebrae in the lumbosacral region and alterations of the forelimb stylopodal skeleton were observed, confirming that mammalian *Hox* genes are involved in the patterning of both axial and appendicular skeletons, as previously revealed by *Hoxa-10* (Rijli et al., 1995, Favier et al., 1996), *Hoxa-11* (Small and Potter, 1993), *Hoxd-11* (Davis and Capecchi, 1994; Favier et al., 1995) and *Hoxd-13* (Dollé et al., 1993) mutations. Furthermore, the analysis of

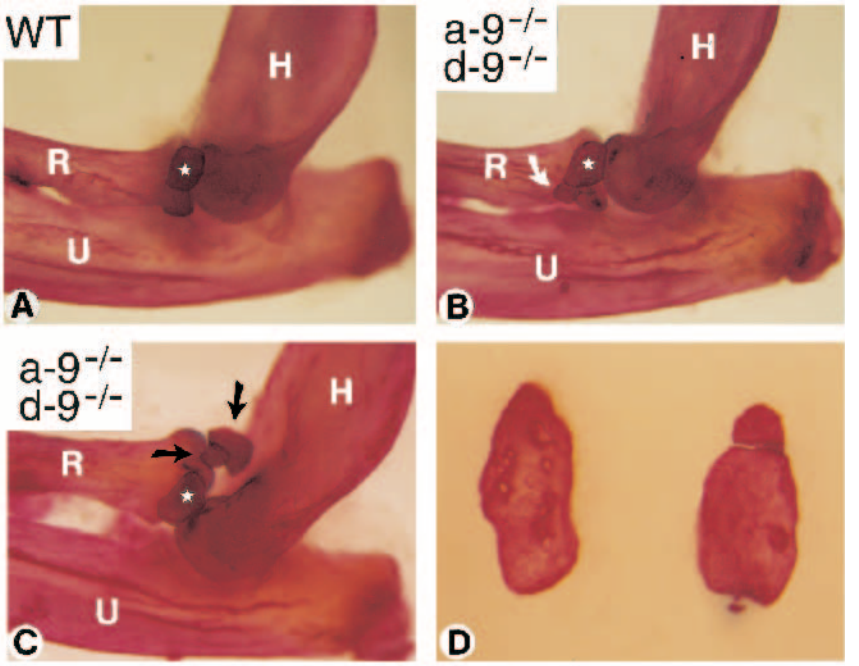


**Fig. 8**. (A-C) Lateral views of the elbow region of a WT (A) and two *Hoxa-9*$^{-/-}$*/Hoxd-9*$^{-/-}$ mutants (B, C). The stars indicate the orthotopic sesamoid bones. White arrow, supernumerary lateral sesamoid; black arrows, large supernumerary ventral sesamoids. Note also that the orthotopic sesamoid bone is enlarged in C. (D) Two dissected supernumerary ventral sesamoids from double homozygous null mutant elbows. Notice that the specimen on the right (which is shown in situ in C) is split in two parts.

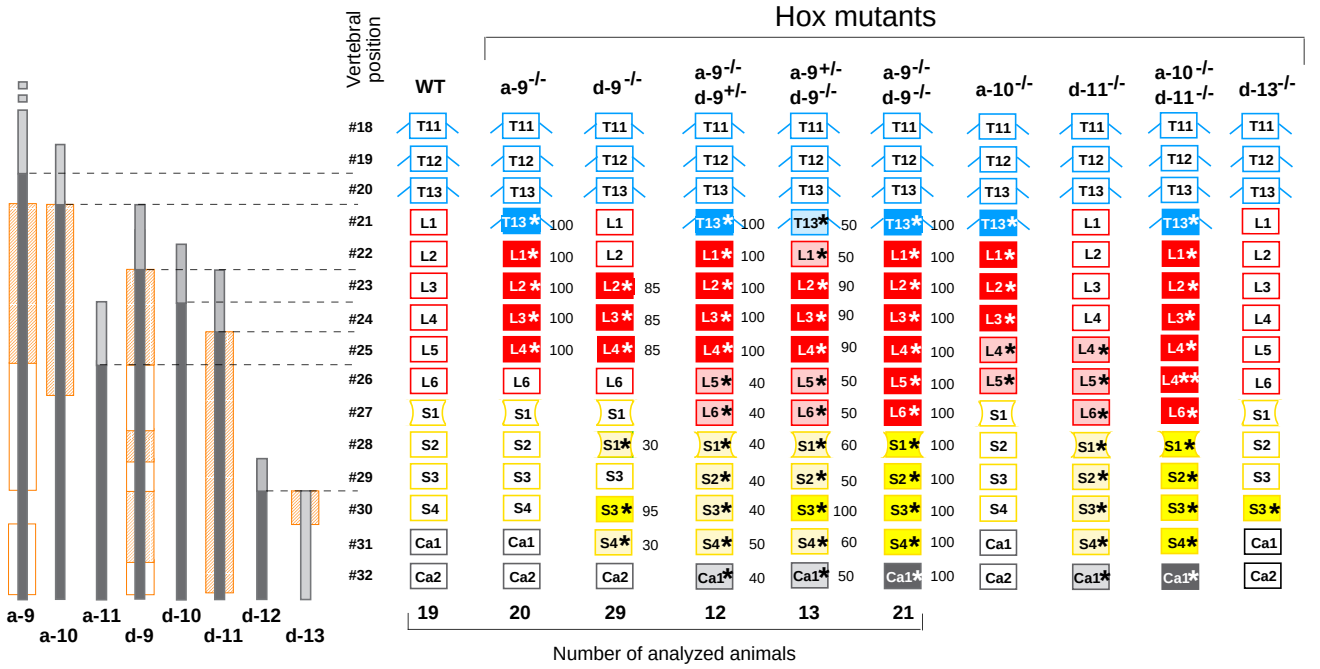


**Fig. 9**. Schematic representation of the morphological anterior transformations of lumbar, sacral and caudal vertebrae in *Hoxa-9*$^{-/-}$, *Hoxd-9*$^{-/-}$, *Hoxa-9*$^{-/-}$/*Hoxd-9*$^{+/-}$, *Hoxa-9*$^{+/-}$/*Hoxd-9*$^{-/-}$, *Hoxa-9*$^{-/-}$/*Hoxd-9*$^{-/-}$, *Hoxa-10*$^{-/-}$, *Hoxd-11*$^{-/-}$, *Hoxa-10*$^{-/-}$/*Hoxd-11*$^{-/-}$ and *Hoxd-13*$^{-/-}$ animals. Data for *Hoxa-10*$^{-/-}$ (Rijli et al., 1995; Favier et al., 1996b), *Hoxd-11*$^{-/-}$ (Davis and Capecchi, 1994; Favier et al., 1995, 1996), and *Hoxd-13*$^{-/-}$ (Dollé et al., 1993) have been previously published. The left side of the figure shows the domains of expression of the *Hoxa* and *Hoxd* genes at 12. 5 dpc, indicated by gray bars, with lighter shading representing the weaker expression level in the most rostral domain. The thoracic vertebrae (T) are depicted in blue, the lumbar (L) in red, the sacral (S) in yellow and the caudal (Ca) in grey. The transformed vertebrae are indicated according to their new morphology and with an asterisk. The vertebrae are uncoloured when they have a WT morphology, intensively coloured when they are transformed with a high penetrance (between 80 and 100%) and lightly coloured when they are transformed with a 30 to 80% penetrance. The numbers on the right side of each transformed vertebrae indicates the penetrance of the transformations in per cent. The orange boxes placed on the expression domains of *Hoxa-9, Hoxa-10, Hoxd-9, Hoxd-11* and *Hoxd-13* indicate the specific (hatched boxes) and redundant (open boxes) functional domains of these genes (see text).

the double mutants reveals a partial functional redundancy between the two genes in the developing vertebral column, as well as in the forelimb. Our results also provide further support to the proposal that specification of the identity of a vertebral segment results from the combinatorial effect of *Hox* genes expressed in that segment (Kessel and Gruss, 1991).

## Functional redundancy between *Hoxa-9* and *Hoxd-9* for development of the forelimb stylopod

The *Hoxd-9* gene displays similar expression pattern in the developing forelimbs and hindlimbs (Dollé and Duboule, 1989). *Hoxd-9* is homogeneously expressed in the undifferentiated mesenchyme of the early limb buds (9.5-10.5 dpc). At later stages, *Hoxd-9* expression becomes progressively restricted to the precartilaginous condensations of the stylopod, while it remains more diffuse in the autopod. By 13.5-14.5 dpc, *Hoxd-9* is specifically expressed in the periphery of the developing humeral and femoral cartilages, and very weakly in more distal regions. *Hoxa-9* expression, which we have studied at 11.5-14.5 dpc (our unpublished results) appears to be very similar to that of *Hoxd-9*. Indeed, *Hoxa-9* transcripts are clearly preferentially expressed around the developing stylopod (humerus and femur) elements, while they are more diffuse in the zeugopod and autopod, with a general decrease in their expression level at 14.5 dpc.

*Hoxa-9* disruption does not result in detectable limb abnormalities, whereas *Hoxd-9* inactivation affect only weakly the P-D growth of the humerus, and mildly the shape of the deltoid crest with a low penetrance. The alterations observed in *Hoxa-9*$^{-/-}$/*Hoxd-9*$^{-/-}$ double mutants, which are almost limited to the forelimb stylopod, are much more severe than the sum of those displayed by either single mutant. The shortening of the humerus and the severe truncation of the deltoid crest can be considered as alterations of the *Hoxd-9*$^{-/-}$ phenotype which are accentuated and more penetrant in double homozygous mutants, thus suggesting a partial functional redundancy between *Hoxa-9* and *Hoxd-9*. In contrast, the alterations of the shape of the humeral head, which are not seen in *Hoxd-9*$^{-/-}$ mutants, indicate that *Hoxa-9* and *Hoxd-9* are fully redundant in this region. Furthermore, there is a dosage effect in the functional compensation between *Hoxa-9* and *Hoxd-9*, as the *Hoxa-9*$^{+/-}$/*Hoxd-9*$^{-/-}$ mutants exhibit abnormalities of the double homozygous mutant phenotype with a lower penetrance and variable expressivity. In contrast, the *Hoxa-9*$^{-/-}$/*Hoxd-9*$^{+/-}$ mutants have apparently normal forelimbs, revealing that *Hoxd-9* is more critical than *Hoxa-9* for proper forelimb morphogenesis, and that the presence of only one functional *Hoxd-9* allele is sufficient in this process.

*Hoxa-9*$^{-/-}$/*Hoxd-9*$^{-/-}$ forelimb abnormalities are restricted to a proximal region encompassing the stylopod and the

elbow. The entire humerus appears to be evenly reduced in size, but most of the morphological alterations (i.e. alterations of characteristic features of the bone) are limited to its proximal part, and therefore to the most proximal region of *Hoxa-9* and *Hoxd-9* expression during development (see above). The *Hoxa-9*$^{-/-}$*/Hoxd-9*$^{-/-}$ phenotype is thus in agreement with the modified principle of functional prevalence of 5′-located *Hox* genes in the distal regions of the developing forelimb (Duboule and Morata, 1994). It is noteworthy that this phenotype has no features resembling a partial homeotic transformation of the humerus. As previously proposed for alterations resulting from *Hoxa-10* (Favier et al., 1996), *Hoxa-11* (Small and Potter, 1993), *Hoxd-11* (Davis and Capecchi, 1994, Favier et al., 1995) or *Hoxd-13* (Dollé et al., 1993) inactivations, the present *Hoxa-9*$^{-/-}$*/Hoxd-9*$^{-/-}$ abnormalities may correspond to a perturbed regulation of the proliferation and/or survival of cells in prechondrogenic condensations.

It has been recently reported (Davis et al, 1995) that *Hoxa-11*$^{-/-}$*/Hoxd-11*$^{-/-}$ double mutant mice have dramatic limb defects not apparent in mice homozygous for either single mutation of these two paralogous genes. Both forelimbs and hindlimbs are affected and the effect of the double mutation is particularly striking in the forelimb, where it results in the almost complete absence of the radius and ulna zeugopodal bones. Since these defects become progressively more severe as more mutant alleles (of either *Hoxa-11* or *Hoxd-11*) are added to the genotype, this limb phenotype was qualified as a 'quantitative' one, in which paralogous *Hox* genes function together to specify limb outgrowth and patterning along the proximodistal axis. In view of their results, and the restriction of the *Hoxd-13*$^{-/-}$ mutant limb phenotype to the autopod (Dollé et al., 1993), Davis et al. (1995) have proposed a quantitative model for *Hox* gene function in limb development, in which the paralogous *Hox* gene from groups 9 to 13 would specify patterns of prechondrogenic condensations along the proximodistal (P-D) limb axis, according to their 3′ to 5′ temporal transcriptional cascade (Izpisúa-Belmonte and Duboule, 1992): the *Hox-9* paralogous genes would specify the scapulum, while the stylopodal, the zeugopodal, and the archipodium and neopodium autopodal bones would be specified by the paralogous gene groups *Hox-10*, *Hox-11*, *Hox-12* and *Hox-13*, respectively (Davis et al., 1995). Our present results do not support this model in two respects. Firstly, *Hoxa-9*$^{-/-}$*/Hoxd-9*$^{-/-}$ double mutants do not exhibit any visible scapulum defects; in contrast, the defects are restricted to the humerus, which suggests that the *Hox-9* paralogous group could be crucial for stylopod patterning. The fact that the humerus is not eliminated in *Hoxa-9*$^{-/-}$*/Hoxd-9*$^{-/-}$ mutants cannot reflect a partial functional compensation by *Hoxc-9*, as this gene is not expressed in the forelimb mesenchyme (Peterson et al., 1994). Such a compensation may be performed by *Hoxb-9*, whose limb pattern of expression is currently unknown. Alternatively, members of both the paralogous groups 9 and 10 may participate in the specification of the stylopod (see below, and Favier et al., 1996)**.** Secondly, in contrast to the *Hoxa-11/Hoxd-11* mutation phenotype, that of *Hoxa-9/Hoxd-9* is clearly not a quantitative one, *Hoxd-9* playing a more critical role than *Hoxa-9*. In any event, it is important to stress that the present partial functional redundancy, which is revealed by knocking out *Hoxa-9* in a *Hoxd-9*$^{-/-}$ genotype, may not reflect the physiological situation. It is conceivable that in the present case (and in other cases of functional redundancies) one *Hox* gene only (here *Hoxd-9*) could be responsible for specification of the structures which are altered in the double mutants (here *Hoxa-9*$^{-/-}$*/Hoxd-9*$^{-/-}$), and that the 'redundant' gene (here *Hoxa-9*) would 'artefactually' replace the physiologically relevant gene only when the latter has been knocked-out.

Interestingly, no alterations could be detected in the hindlimbs of *Hoxa-9*$^{-/-}$*/Hoxd-9*$^{-/-}$ mutant mice, even though both genes are similarly expressed in developing forelimbs and hindlimbs. This may reflect a functional redundancy with the *Hoxc-9* gene which is expressed in hindlimb, but not forelimb mesenchyme (Peterson et al., 1994). *Hoxb-9* (see above) is also a possible candidate for functional compensation. Additionally, genes of the paralogous group 10 may be more critical for hindlimb than for forelimb patterning, since *Hoxa-10* gene knock-out markedly affects the femur and the knee, even though this gene is similarly expressed up to proximal regions of the developing femur and humerus (Favier et al., 1996). Additional compound mutations are required to further evaluate the role of genes of the paralogous groups 9 and 10 in forelimb and hindlimb development.

### Specific and redundant functional domains of *Hoxa-9* and *Hoxd-9* for axial skeleton specification in the lumbosacral region

WT mice have 7 cervical, 13 thoracic, 6 lumbar, 4 sacral and a variable number of caudal vertebrae (7C/13T/6L/4S phenotype) (see Fig. 9). *Hoxa-9*$^{-/-}$ mutants exhibit 14 thoracic and 5 lumbar vertebrae (7C/14T/5L/4S phenotype), with anterior transformations of vertebra #21 (WT L1) to a thoracic morphology (T13*), and of vertebrae #22 to #25 (WT L2 to L5) towards L1* to L4* morphologies (Fig. 9). *Hoxd-9*$^{-/-}$ mutants present anterior transformations of 3 lumbar vertebrae (#23, #24 and #25 to L2*, L3* and L5* morphologies) and 2 sacral and caudal vertebrae (#28 and #30, #31 to S1* and S3*, S4* morphologies), while vertebrae #26, #27 and #29 exhibit a L6, S1 and S3 morphology, respectively, as in WT animals (Fig. 9). These transformations are in keeping with the other anterior homeotic transformations along the axial skeleton, which have been previously reported for several *Hox* gene loss-of-function mutations (Krumlauf, 1994 and refs. therein).

Vertebra #30 (WT S4) appears to be anteriorly transformed to an S3 morphology (S3*) in *Hoxd-9*$^{-/-}$ mutants, based mainly upon the presence of 4 fused vertebrae in the sacrum of these mutants, instead of 3 fused vertebrae (S1 to S3) in most heterozygotes and WT littermates. Dollé et al. (1993) have proposed that the fusion of the transverse processes, which are observed between the 3rd and 4th sacral vertebrae in *Hoxd-13* mutants (S3 and S3*, Fig. 9), may not correspond to a genuine anterior transformation of S4, but be related to a reduction of the posterior half of the mutant S3 vertebral body. The transverse processes would then come into contact and fuse. However, there is a complete fusion of the transverse processes of vertebrae #29 and #30 (WT S3 and S4), even in the case of a 'mild' *Hoxd-9*$^{-/-}$ phenotype without any reduction of vertebra #29 body (Fig. 4B). Thus, we believe that the fusion seen between vertebrae #29 and #30 in *Hoxd-9*$^{-/-}$ mutants is likely to reflect an anterior homeotic transformation of vertebra #30 (WT S4) to an S3 morphology (S3*) (Fig. 9). In this

respect, it is interesting to note that the 4 sacral vertebrae are normally fused in the rat (Hebel and Stromberg, 1986).

The 90-100% penetrance of the anterior transformations observed in *Hoxa-9*$^{-/-}$ mutants indicates a specific function of *Hoxa-9* in the patterning of the lumbar region encompassing vertebrae #21 to #25 (WT L1 to L5). Similarly, *Hoxd-9* appears to play a distinct role in the specification of vertebrae #23, #24, #25 and #30 (WT L3, L4, L5 and S4). *Hoxd-9* appears also to have a distinct function in the specification of vertebrae #28 and #31 (WT S2 and Ca1), but there is a clear partial functional redundancy with *Hoxa-9* at these levels, as indicated by the full penetrance of the anterior transformations in *Hoxa-9*$^{-/-}$*/Hoxd-9*$^{-/-}$ double mutants (Fig. 9). In addition *Hoxa-9* and *Hoxd-9* appear to be fully redundant and functionally equivalent (compare *Hoxa-9*$^{-/-}$*/Hoxd-9*$^{+/-}$ and *Hoxa-9*$^{+/-}$*/Hoxd-9*$^{-/-}$ in Fig. 9) for the specification of vertebrae #26, #27, #29 and #32 (WT L6, S1, S3 and Ca2). Thus, the domain of activity of the two paralogous genes *Hoxa-9* and *Hoxd-9* is larger than that which is defined by the single mutant phenotypes. Note that both partial and full redundancies are dosage-dependent, since both *Hoxa-9*$^{-/-}$*/Hoxd-9*$^{+/-}$ and *Hoxa-9*$^{+/-}$*/Hoxd-9*$^{-/-}$ mutants can exhibit the same anterior transformations as the homozygous double mutants, albeit with a lower penetrance and variable expressivity. Curiously, the variations in expressivity are not stochastic, since 85-90% of the asymmetric vertebral transformations preferentially occur on the left side.

Taken altogether our results reveal an unexpected complexity in the specification of the vertebral identity in the lumbosacral-caudal region by the two paralogous *Hoxa-9* and *Hoxd-9* genes. In that respect, 4 vertebra groups can be defined (Fig. 9, Table 1): group A (vertebrae #21 and #22, WT L1 and L2), where *Hoxa-9*, but not *Hoxd-9* is required; group B (vertebra #30, WT S4), where only *Hoxd-9*, but not *Hoxa-9* is required; group C (vertebrae #23, #24 and #25, WT L3, L4 and L5) where both *Hoxa-9* and *Hoxd-9* are required, in agreement with a combinatorial model (Kessel and Gruss, 1991) for *Hox* gene function; group D (vertebrae #26, #27, #28, #29, #31 and #32, WT L6, S1, S2, S3, Ca1 and Ca2) where *Hoxa-9* and *Hoxd-9* appear to be partially or fully redundant. As discussed above in the case of the limbs, it is unknown whether these redundancies reflect a physiological situation in which the two genes similarly exert the same patterning function or result from the 'artefactual' new conditions created by the mutations, one of the two genes only being physiologically relevant.

### *Hox* genes and axial skeleton patterning

Fig. 9 and Table 1 summarize the effect of *Hoxa-9* and *Hoxd-9* single and double mutations, as well as those of other *Hox* genes that are expressed in the same region, on the phenotype of the lumbosacral vertebrae and the deduced involvement of these genes in the specification of these vertebrae. From these comparisons, it appears that the current hypotheses and models aimed at explaining how *Hox* genes pattern the axial skeleton must be refined to take into account the complexity which is emerging from combination mutant phenotypes.

The posterior prevalence model (Duboule, 1991) assumes that there is functional hierarchy among vertebrate *Hox* genes similar to that seen in *Drosophila*. In this model, *Hox* genes have a dominant function from the level of their anterior limit of expression to the anterior limit of expression of more posterior (5′-located) *Hox* genes expressed in the same region. Thus, *Hox* gene loss-of-function mutations should result in vertebral transformations only at the level of their rostral domain of expression, and not in regions where more posterior genes are expressed. The vertebral phenotypes of *Hoxa-9*, *Hoxd-9*, *Hoxa-10* and *Hoxd-11* mutants are inconsistent with this prediction of the posterior prevalence model. Note that the faint expression of *Hoxd-9* at the level of vertebrae #21 and #22 is not correlated with a non-redundant specifying function. That the strong expression of *Hoxa-9* at the level of vertebra #20 (WT T13) is not correlated with anterior homeosis of this vertebra may reflect a functional redundancy between *Hoxa-9* and another *Hox* gene expressed at this level (e.g. *Hoxc-9*).

The posterior prevalence model has been modified recently to incorporate a quantitative aspect, in which the relative amounts of *Hox* proteins may play an important role in determining the functional hierarchy in the specification of vertebra identity (Duboule and Morata, 1994). It is hypothesized that the effect of a more anterior gene may be predominant in its entire domain of high expression. The *Hoxa-9*$^{-/-}$ phenotype, as well as the *Hoxa-10*$^{-/-}$ phenotype, might be consistent with this quantitative model. However, it is inconsistent with the *Hoxd-11*$^{-/-}$ phenotype, as well as with the *Hoxd-9*$^{-/-}$ phenotype in which vertebrae #26, #27 and #29 are unaffected, whereas vertebrae #23 to #25, #28 and #30 are transformed. Note in this respect that there is no visible variations in the level of *Hoxd-9* transcripts in the region encompassing vertebrae #23-#32 (our unpublished data). The phenotypes of the double mutants *Hoxa-9/Hoxd-9* and *Hoxa-10/Hoxd-11* are also inconsistent with the quantitative posterior prevalence model, since in both cases all of the vertebrae caudal to vertebrae #25-#26 are similarly anteriorly transformed, even though there are several more posterior genes strongly expressed in this region. In this respect, it is also worth noting that the double mutants *Hoxa-9*$^{-/-}$*/Hoxd-9*$^{-/-}$ and *Hoxa-10*$^{-/-}$*/Hoxd-11*$^{-/-}$ have a similar phenotype with an anterior transformation of all vertebrae from position #21 to #32 (for further discussion, see Favier et al., 1996). The study of additional combination mutant phenotypes will establish whether the identity of a given vertebra is specified by the combination of most if not all of the *Hox* genes that are expressed at its level, whether paralogous or non-paralogous, and irrespective of their anterior limit of expression. In this respect, it will be important to check whether the levels of Hox gene transcripts discussed here reflect the abundance of the corresponding proteins.

It has also been suggested that *Hox* genes might cooperate in the patterning of vertebrae by separately specifying different morphological structures of the same vertebrae (Krumlauf, 1994; Pollock et al., 1995). In this respect, we did not notice any clear-cut differences in the aspects of the transformed vertebrae, whether the transformation resulted from a single or a double mutation, and whether it originated from *Hoxa-9*, *Hoxd-9*, *Hoxa-10* or *Hoxd-11* mutations (see Table 1). This suggests that, at least in the lumbosacral region, there is no morphological 'division of labour' between the different *Hox* genes that participate in the specification of a vertebra, but rather that several genes extensively cooperate in the proper specification of many aspects of vertebral morphology. Clearly, our results support a combinatorial model of vertebral patterning by the *Hox* genes co-expressed in a given region (Kessel and Gruss, 1991). Analysis of Hox proteins at the single-cell level is a prerequisite to establish whether this coop-

erativity could be achieved through transcriptional control of the same downstream genes or through parallel pathways, possibly in different cells of a prevertebral segment, in a cell autonomous or non-autonomous way.

We dedicate the present study to the memory of the late Dr Sudhakar Lakkaraju, who performed the initial part of *Hoxa-9* study. We thank Professor P. Gruss for his support, Dr S. Ward for a critical reading of the manuscript, M. LeMeur and her staff for the animal facilities and blastocysts injection, D. Queuche and J. M. Kuhry for technical assistance in ES cell culture. This work was supported by funds from the Institut National de la Santé et de la Recherche Médicale, the Centre National de la Recherche Scientifique, the Centre Hospitalier Universitaire Régional, the Association pour la Recherche sur le Cancer (ARC), and the Fondation pour la Recherche Médicale (FRM). B. F. was supported by a fellowship from la Ligue Nationale contre le Cancer.

## REFERENCES

**Condie, B. G. and Capecchi, M. R.** (1994). Mice with targeted disruptions in the paralogous genes *Hoxa-3* and *Hoxd-3* reveal synergistic interactions. *Nature* **370**, 304-307.

**Davis, A. P. and Capecchi, M. R.** (1994). Axial homeosis and appendicular skeleton defects in mice with a targeted disruption of *Hoxd-11*. *Development* **120**, 2187-2198.

**Davis, A. P., Witte, D. P., Hsieh-Li, H. M., Potter, S. S. and Capecchi, M. R.** (1995). Absence of radius and ulna in mice lacking *Hoxa-11* and *Hoxd-11*. *Nature* **375**, 791-795.

**Dollé, P. and Duboule, D.** (1989). Two gene members of the murine *HOX-5* complex show regional and cell-type specific expression in developing limbs and gonads. *EMBO J.* **8**, 1507-1515.

**Dollé, P., Izpisúa-Belmonte, J. C., Falkenstein, H., Renucci, A. and Duboule, D.** (1989). Coordinate expression of the murine *Hox-5* complex homeobox-containing genes during limb pattern formation. *Nature* **342**, 767-772.

**Dollé, P., Izpisúa-Belmonte, J. C., Brown, J. M., Tickle, C. and Duboule, D.** (1991). *Hox-4* genes and the morphogenesis of mammalian genitalia. *Genes Dev*. **5**, 1767-1776.

**Dollé, P. and Duboule, D.** (1993). Structural and functional aspects of mammalian *Hox* genes. *Adv. Dev. Biochem.* **2**, 55-106.

**Dollé, P., Dierich, A., LeMeur, M., Schimmang, T., Schuhbaur, B., Chambon, P. and Duboule, D.** (1993). Disruption of the *Hoxd-13* gene induces localized heterochrony leading to mice with neotenic limbs. *Cell* **75**, 431-441.

**Duboule, D. and Dollé, P.** (1989). The structural and functional organization of the murine *HOX* gene family resembles that of *Drosophila* homeotic genes. *EMBO J.* **8**, 1497-1505.

**Duboule, D.** (1991). Patterning in the vertebrate limb. *Current Op. Genetics Dev.* **1**, 211-216.

**Duboule, D. and Morata, G.** (1994). Colinearity and functional hierarchy among genes of the homeotic complexes. *Trends Genet.* **10**, 358-364.

**Favier, B., LeMeur, M., Chambon, P. and Dollé, P.** (1995). Axial skeleton homeosis and forelimb malformations in *Hoxd-11* mutant mice. *Proc. Natl. Acad. Sci. USA* **92**, 310-314.

**Favier, B., Rijli, F. M., Fromental-Ramain, C., Fraulob, V., Chambon, P. and Dollé P.** (1996) Functional cooperation between the non-paralogous genes *Hoxa-10* and *Hoxd-11* in the developing forelimb and axial skeleton. *Development* **122**, 449-460.

**Gossler, A., Doetschman, T., Korn, R., Serfling, E. and Kemler, R.** (1986). Transgenesis by means of blastocyst-derived embryonic stem cell lines. *Proc. Natl. Acad. Sci. USA* **83**, 9065-9069.

**Haack, H. and Gruss, P.** (1993). The establishment of murine *Hox-1* expression domains during patterning of the limb. *Dev. Biol.* **157**, 410-422.

**Hebel, R. and Stromberg, M. W.** (1986) Anatomy and embryology of the laboratory rat. *BioMed. Verlag., Germany*.

**Izpisúa-Belmonte, J. C. and Duboule, D.** (1992) Homeobox genes and pattern formation in the vertebrate limb. *Dev. Biol.* **152**, 26-36.

**Kessel, M., Balling, R., and Gruss, P.** (1990). Variations of cervical vertebrae after expression of a *Hox-1. 1* transgene in mice. *Cell* **61**, 301-308.

**Kessel, M. and Gruss, P.** (1991). Homeotic transformations of murine vertebrae and concomitant alteration of *Hox* codes induced by retinoic acid. *Cell* **67**, 89-104.

**Krumlauf, R.** (1994). *Hox* genes in vertebrate development. *Cell* **78**, 191-201

**Lufkin, T., Mark, M., Hart, C. P., Dollé, P., Lemeur, M. and Chambon, P.** (1992). Homeotic transformation of the occipital bones of the skull by ectopic expression of a homeobox gene. *Nature* **359**, 835-841.

**McGinnis, W. and Krumlauf, R.** (1992). Homeobox genes and axial patterning. *Cell* **68**, 283-302.

**Morgan, B. A., Izpisúa-Belmonte, J. C., Duboule, D. and Tabin, C.** (1992). Targeted misexpression of *Hox-4. 6* in the avian limb bud causes apparent homeotic transformations. *Nature* **358**, 236-239.

**Peterson, R. L., Papenbrock, T., Davda, M. M. and Awgulewitsch, A.** (1994). The murine *HOXC* cluster contains five neighboring *AbdB*-related *Hox* genes that show unique spatially coordinated expression in posterior embryonic subregions. *Mech. Dev.* **47**, 253-260.

**Pollock, A. R., Sreenath, T., Ngo, L. and Bieberich, C. J.** (1995) Gain of function mutations for paralogous *Hox* genes: implications for the evolution of *Hox* gene function. *Proc. Natl. Acad. Sci. USA* **92**, 4492-4496.

**Rijli, F. M., Dollé, P., Fraulob, V., LeMeur, M. and Chambon, P.** (1994). Insertion of a targeting construct in a *Hoxd-10* allele can influence the control of *Hoxd-9* expression. *Dev. Dynamics* **201**, 366-377.

**Rijli, F., Matyas, R., Pellegrini, M., Dierich, A., Gruss, P., Dollé, P. and Chambon, P.** (1995). Cryptorchidism and homeotic transformations of spinal nerves and vertebrae in *Hoxa-10* mutant mice. *Proc. Natl. Acad. Sci. USA* **92**, 8185-8189.

**Ruddle, F. H., Bartels, J. L., Bentley, K. L., Kappen, C., Murtha, M. T. and Pendelton, J. W.** (1994). Evolution of *Hox* genes. *Annu. Rev. Genet.* **28**, 423-442.

**Scott, M. P.** (1992). Vertebrate homeobox gene nomenclature. *Cell* **71**, 551-553.

**Small, K. M. and Potter, S. S.** (1993). Homeotic transformations and limb defects in *Hoxa-11* mutant mice. *Genes Dev.* **7**, 2318-2328.

**Suemori, H., Takahashi, N. and Noguchi, S.** (1995) *Hoxc-9* mutant mice show anterior transformation of the vertebrae and malformation of the sternum and ribs. *Mech. Dev.* **51**, 265-273.

**Thomas, K. R. and Capecchi, M. R.** (1987). Site-directed mutagenesis by gene targeting in mouse embryo-derived stem cells. *Cell* **51**, 503-512.

(Accepted 22 November 1995)